





Probing uniform and nonuniform charge ordering with polarized femtosecond optical pulses in geometrically frustrated θ -(BEDT-TTF)₂MZn(SCN)₄ ($M = \text{Rb}, \text{Cs}$)

K. Nakagawa ¹, S. Tsuchiya ^{1,*}, H. Taniguchi ² and Y. Toda ¹

¹Department of Applied Physics, Hokkaido University, Sapporo, Hokkaido, 060-8628, Japan

²Graduate School of Science and Engineering, Saitama University, Saitama, 338-8570, Japan



(Received 4 August 2022; accepted 8 December 2022; published 19 January 2023)

In this work, we investigated polarization-resolved photoinduced carrier relaxation dynamics associated with charge ordering (CO) in geometrically frustrated organic conductors θ -(BEDT-TTF)₂MZn(SCN)₄ ($M = \text{Rb}, \text{Cs}$) as a function of temperature. In θ -Rb ($M = \text{Rb}$), a polarization-dependent (anisotropic) and independent (isotropic) dynamics show similar temperature dependence. Moreover, discontinuous changes in transient reflectivity amplitude and an enhancement of a relaxation time are observed only upon heating near $T_{\text{co}} = 195$ K. This is associated with the first order phase transition due to long-range CO. However, in θ -Cs ($M = \text{Cs}$) where the frustration is stronger than that in θ -Rb, as temperature decreases below $T_{\text{nco}} \approx 150$ K, the anisotropic component only slightly decreases while the isotropic one increases gradually without hysteresis. The behaviors indicate that CO is formed nonuniformly, that is, multiple short-range CO domains appear and are distributed with different orientations. Moreover, we found that the anisotropic dynamics with long-relaxation times suppress below $T_s \approx 50$ K, which is lower than the charge glass transition temperature of $T_g \sim 100$ K, whereas the isotropic dynamics grows monotonically. The distinct difference between them suggests the occurrence of a structural transition in which the lattice deforms randomly to match a glassy charge distribution due to the charge-lattice coupling.

DOI: [10.1103/PhysRevResearch.5.013024](https://doi.org/10.1103/PhysRevResearch.5.013024)

I. INTRODUCTION

Optical pump-probe time-resolved spectroscopy has been conducted to study chemical reactions [1], dynamics of photoexcited carriers in semiconductors [2], and photoinduced phase transitions [3,4]. Remarkably, in strongly correlated electron systems, relaxation processes of photoinduced carriers have provided new insights into the mechanism of correlation-driven phase transitions. Up to now, this technique has been applied to various correlated materials, such as cuprates [5–9], pnictides [10,11], and organic superconductors [12,13].

Among strongly correlated materials, organic charge transfer salts θ -(BEDT-TTF)₂MZn(SCN)₄ ($M = \text{Rb}, \text{Cs}$) have been of great interest, where BEDT-TTF denotes bis(ethylenedithio)tetrathiafulvalene, because the frustration of the charge distribution in the triangular crystal lattice plays an important role for nature of the conducting electrons [14,15]. In θ -Rb ($M = \text{Rb}$), stripe-type charge ordering (CO) in long range has been suggested as an insulating ground state below $T_{\text{co}} = 195$ K when the sample is slowly cooled [16,17]. However, on fast cooling in θ -Rb or in θ -Cs ($M = \text{Cs}$), which has a stronger charge frustration than that

in θ -Rb, has shown no CO transition, and, instead, multiple short-range COs and glassy charge dynamics have been observed, indicating realization of CG state [18,19]. The CG state has been extensively studied by various experiments to reveal the universality and diversity of glass state. However, the nonequilibrium carrier relaxation process in the CO and CG states has not yet been identified.

An ultrafast optical pump probe spectroscopy is a major technique for investigating the relaxation process of photoexcited carriers. In a CDW state of DyTe₃ [20] which has a similar spatial electronic structure to the CO state, the CDW transition has been characterized by carrier relaxation dynamics that depend on probe polarization. Moreover, in an organic superconductor, this measurement has successfully probed a small superconducting (SC) gap due to fluctuation in the SC order parameter as well as bulk SC gaps [21,22]. Therefore, by applying the pump probe measurement technique to the frustrated CO system, not only the relaxation process of long-range CO, but also short-range and more complex CO formations can be explored.

In this paper, we investigate the relaxation dynamics of photoinduced carriers associated with CO formations in charge frustrated organic conductors θ -Rb and θ -Cs by polarized pump probe spectroscopy measurements with varying temperature. In θ -Rb, both polarization-dependent (anisotropic) and polarization-independent (isotropic) transient signal increase below T_{co} during cooling and heating. Moreover, the abrupt changes in the amplitude and the relaxation time are observed near T_{co} only in the heating process, indicating that the first-order phase transition due to the long-range CO occurs. In θ -Cs, we find two characteristic

*satoshi.tsuchiya@eng.hokudai.ac.jp

Published by the American Physical Society under the terms of the Creative Commons Attribution 4.0 International license. Further distribution of this work must maintain attribution to the author(s) and the published article's title, journal citation, and DOI.

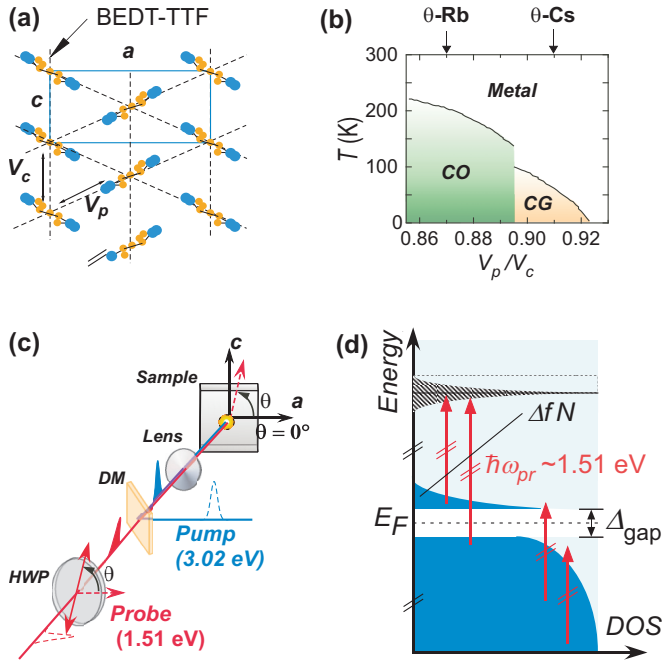


FIG. 1. (a) A schematic illustration of arrangement of BEDT-TTF molecules. V_c and V_p are intersite Coulomb energies. (b) A conceptual phase diagram of θ -(BEDT-TTF) $_2$ MZn(SCN) $_4$ ($M = \text{Rb}$ and Cs) as a function of V_p/V_c under the slow cooling condition (<1 K/min) [23,24]. CO and CG denote the charge order, and charge glass, respectively. (c) A schematic view of the measurement setup for polarized pump probe spectroscopy. HWP and DM stand for a half-wave plate and dichroic mirror, respectively. (d) A schematic illustration of possible optical transitions in the probe process after pump excitation. DOS and Δ_{gap} denote the electronic density of states and the energy gap, respectively.

temperatures. One is $T_{\text{hco}} \approx 150$ K at which the anisotropic dynamics does not change but the isotropic dynamics increases monotonically. The behavior suggests that multiple short-range CO domains appear with different orientations. The other is $T_s \approx 50$ K, which is lower than the CG transition temperature of $T_g \sim 100$ K. Below T_s , anisotropic dynamics with long relaxation times suppress, indicating the occurrence of a novel structural transition in which the lattice is modulated to match the inhomogeneous charge distribution in the CG state due to charge-lattice coupling.

II. EXPERIMENTAL

Single crystals of θ -Rb and θ -Cs were synthesized electro chemical oxidation method [16]. As shown in Fig. 1(a), BEDT-TTF molecules are arranged on an anisotropic triangular lattice, forming a conducting layer. The conducting layers are alternately stacked with insulating layer of $\text{CsZn}(\text{SCN})_4$ along the b axis. Figure 1(b) shows the temperature (T) versus V_p/V_c phase diagram under slow cooling conditions (<1 K/min) [23,24], where V_c and V_p are intersite Coulomb energies shown in Fig. 1(a). V_p/V_c corresponds to a measure of charge frustration. θ -Rb undergoes the long-range CO transition at $T_{\text{co}} = 195$ K. θ -Cs which has the V_p/V_c value than that of θ -Rb, shows no CO transition but the several

experimental studies have suggested that two kinds of short-range CO grow [25], leading to nonequilibrium glassy dynamics above the glass transition temperature $T_g \approx 100$ K [18]. In the study, T_g is kinetic origin and determined by an empirical definition in conventional glass studies [18].

Figure 1(c) shows the schematic view of the measurement setup. Optical pulses of 120 fs was obtained from a cavity dumped mode-lock Ti:Al $_2$ O $_3$ oscillator and a repetition rate was set to 11 kHz to avoid the heating effect. Pulses centered at 3.02 eV, which were obtained by frequency doubling in a LiB $_3$ O $_5$ (LBO) crystal, were used for pump and pulses at 1.51 eV were used for probe. Pump and probe pulses were coaxially overlapped and irradiated perpendicular to the conducting plane. To measure a probe polarization dependence, a probe polarization was changed by rotation of a half wave plate (HWP). The θ is a polarization angle measured from the a axis. Beam spot sizes of the pump and probe were ~ 20 μm and ~ 12 μm in diameter, respectively. Fluence of pump pulse was fixed to ~ 100 – 110 $\mu\text{J}/\text{cm}^2$ during the measurements. This fluence is close to the threshold value ~ 90 – 100 $\mu\text{J}/\text{cm}^2$ at which the signal amplitude deviates slightly from the linear variation in the fluence-dependence measurement at $T = 60$ K in θ -Rb.

The data were obtained during heating and cooling processes. In the heating process, firstly sample was cooled to low temperatures with a rate of 0.5 K/min., which was sufficient to cause the CO transition in θ -Rb, and then a measurement was carried out with increasing temperature. In the cooling process, the data were obtained with decreasing temperature from a room temperature. In this case, an averaged cooling rate is less than ~ 0.5 K/min.

In the pump probe measurements, the carriers excited by the pump pulse relax and accumulate the electronic states near the Fermi energy by electron-electron and electron-phonon scattering, forming nonequilibrium distribution of carriers as well as phonons [26]. In general, nonequilibrium electronic temperature increases by a few K [27]. The probe pulse measures a transient change in reflectivity $\Delta R/R$ which is associated with optical transitions between photoexcited carrier states near E_F and unoccupied states above the probe energy, and transitions between unoccupied states near E_F and occupied states below the probe energy as shown in Fig. 1(d). Based on the Fermi's golden rule, $\Delta R/R$ is described as

$$\frac{\Delta R}{R} = \frac{R_{\text{pump}} - R_0}{R_0} \propto \Delta f N |\mathbf{M}|^2, \quad (1)$$

where R_{pump} and R_0 denote the reflectivities with and without pump pulse irradiation, respectively, and Δf and N are the nonequilibrium distribution function of carriers, the density of electronic states, respectively. \mathbf{M} is written as $\mathbf{M} = \sum_{i,j} b_i M_{ij} a_j$, where M_{ij} denotes the dipole matrix element. As $\Delta R/R$ is measured with varying a delay between pump and probe pulses, the temporal evolution of Δf can be investigated. When an energy gap (Δ_{gap}) exists for electronic excitations, such as an insulating gap due to the CO transition, a relaxation bottleneck may occur and the carrier dynamics may change significantly from the normal state [27,28]. Since, in general, gap amplitude is several tens or hundreds of meV which are quite smaller than the probe energy, the gap itself is not directly observed (as in resonance) in this measurement.

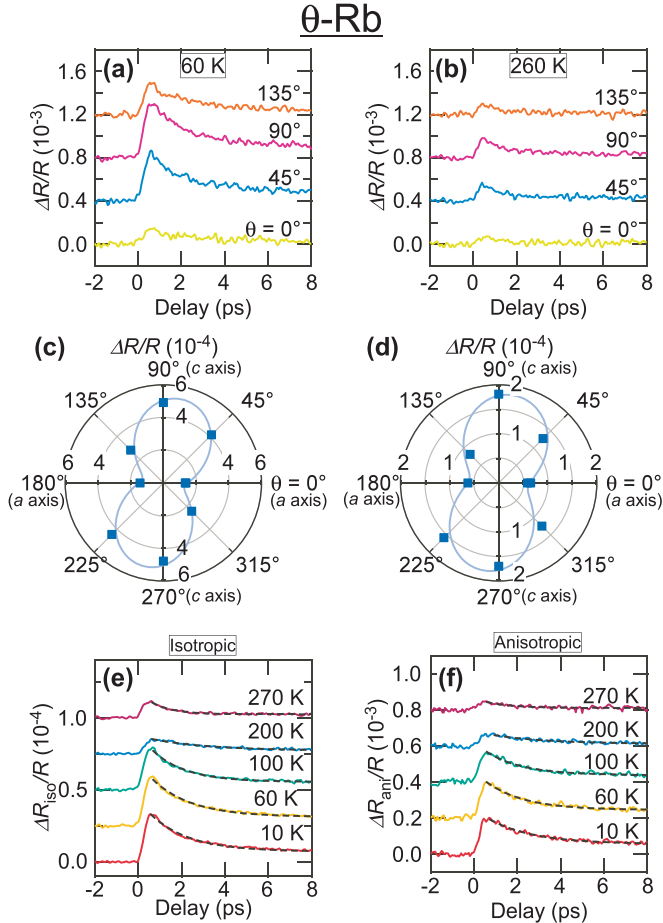


FIG. 2. (a, b) Transient change of reflectivity $\Delta R/R$ for $\theta = 0^\circ$, 45° , 90° , and 135° at $T = 60$ K and 260 K, respectively, in θ -Rb. The data are shifted for clarity. (c, d) Polar plots of the amplitude of $\Delta R/R$ as a function of θ at $T = 60$ K and 260 K, respectively. The signal amplitude is defined as the $\Delta R/R$ value at 0.5 ps. The solid lines denote the results fitted by Eq. (2). (e, f) $\Delta R_{\text{iso}}/R$ and $\Delta R_{\text{ani}}/R$, respectively, at $T = 10, 60, 100, 200,$ and 270 K. The data are shifted for clarity.

Nevertheless, the carrier distribution (Δf) induced by the pump pulse varies with the presence or absence of a gap, temperature, and delay time. Therefore, we can extract information on low-energy electronic structures at the E_F through dynamics measurements.

The probe polarization anisotropy appears in M in Eq. (1). Thus, when an anisotropic change in the electronic state near the Fermi energy occurs, polarization anisotropy is expected to appear in $\Delta R/R$. We note that the polarization anisotropy is a consequence of the anisotropy of M_{ij} regarding the optical transitions indicated by the red arrows in Fig. 1(d). In this sense, the probe anisotropy is not directly related to the low-energy electronic gap structure [29,30].

III. RESULTS

First, we show the results of θ -Rb. Figures 2(a) and 2(b) show the transient change of reflectivity ($\Delta R/R$) for $\theta = 0^\circ$, 45° , 90° , and 135° at $T = 60$ K and 260 K, respectively, in

θ -Rb on heating. At $T = 260$ K, $\Delta R/R$ changes depending on θ . At $T = 60$ K, the signal amplitude of $\Delta R/R$ at each θ values seems to increase as compared to those at $T = 260$ K. Figures 2(c) and 2(d) show polar plots of the amplitude of $\Delta R/R$ at $T = 60$ K and 260 K, respectively. At $T = 260$ K, the signal is enhanced along the c axis and the direction of the polarization anisotropy is kept at $T = 60$ K. The slight difference between the crystal axis and the probe polarization is due to misalignment.

For further analysis, the data are decomposed into polarization-independent (isotropic) and polarization-dependent (anisotropic) components by fitting the following equation:

$$\frac{\Delta R}{R}(\theta) = \frac{\Delta R_{\text{iso}}}{R} + \frac{\Delta R_{\text{ani}}}{R} \cos(2\theta - 2\theta_0), \quad (2)$$

where $\Delta R_{\text{iso}}/R$ and $\Delta R_{\text{ani}}/R$ are isotropic and anisotropic transients, respectively, and θ_0 corresponds to a direction where the transient signal is most enhanced. The fitting was carried out at each delay time and the decomposed data are replotted as a function of temperature in Figs. 2(e) and 2(f). The signal amplitude seems to increase with decreasing temperature for both isotropic and anisotropic components. The θ_0 values are $\sim 80^\circ$ at any delay time and are independent of temperature.

To see temperature dependencies of the carrier dynamics in more detail, the transient signal amplitude in the isotropic (anisotropic) component of A_{iso} (A_{ani}) and the relaxation time of τ_{iso} (τ_{ani}) are estimated by fitting with a single exponential function $A_{\text{iso}} \exp(-t/\tau_{\text{iso}}) + C_{\text{iso}}$ ($A_{\text{ani}} \exp(-t/\tau_{\text{ani}}) + C_{\text{ani}}$), where C_{iso} (C_{ani}) is a component with infinite relaxation time. The fitting results are shown as the dashed lines in Figs. 2(e) and 2(f). The temperature dependencies of A_{iso} and A_{ani} on heating for θ -Rb are shown in Fig. 3(a). As temperature increases from below, A_{iso} and A_{ani} gradually decrease and steeply decrease at around 160 K and increase at $T_{\text{co}} = 195$ K. Since T_{co} almost corresponds to the temperature at which a metal-insulator transition [16] and a structural phase transition [31–33] occur, the temperature-dependent changes in A_{iso} and A_{ani} indicate the CO transition. Here, the isotropic and anisotropic dynamics reflect amplitude of the CO and anisotropy in the electronic structure induced by the CO transition, respectively. The validity of the above correspondences will be discussed later. We note that our main results are not affected even if the analysis is based on a double exponential function.

Figure 3(b) shows the temperature dependencies of the τ_{iso} and τ_{ani} . The τ_{iso} and τ_{ani} values between 160 and 195 K are found to be larger than those at other temperatures and are most enhanced just below T_{co} . The steep changes in τ_{iso} and τ_{ani} are reminiscent of a divergent behavior of relaxation times near the SC and CDW transition temperatures [20,30], suggesting a phonon bottleneck effect in the photoinduced carrier relaxation.

Figures 3(d) and 3(e) show the temperature dependencies of A_{iso} and A_{ani} and τ_{iso} and τ_{ani} on cooling, respectively. In contrast to the heating process, the discontinuous changes at 160 and 195 K are absent. Moreover, τ_{iso} and τ_{ani} only show a monotonic increase below T_{co} . This hysteresis between the heating and cooling processes indicates a first-order phase

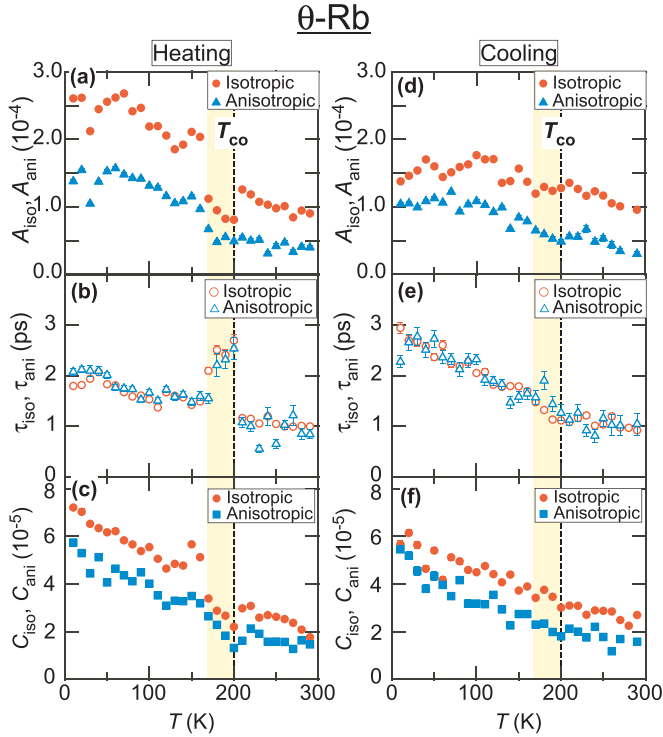


FIG. 3. (a, b, c) Temperature dependencies of A_{iso} , A_{ani} and τ_{iso} , τ_{ani} and C_{iso} , C_{ani} , respectively, on heating in θ -Rb. These on cooling are shown in panels (d, e, f).

transition, consistent with the previous report [33]. Therefore, it is reasonable to consider that the fast-decay dynamics with pronounced hysteresis near T_{co} is attributed to the CO transition.

Figure 3(c) shows the temperature dependence of C_{iso} and C_{ani} on heating. Step changes in C_{iso} and C_{ani} below T_{co} are similar to those in A_{iso} and A_{ani} . Moreover, as shown in Fig. 3(f), both C_{iso} and C_{ani} increases monotonically without steep change below T_{co} on cooling. Thus, the similarity between the temperature dependencies of C_{iso} (C_{ani}) and A_{iso} (A_{ani}) indicates that the formation of the long-range CO contributes not only to the fast decay component but also the long-lived component ($\tau > 8$ ps). As will be discussed later, the behavior of the long-lived component is reasonably interpreted as changes in the electronic structure caused by the lattice distortion due to the CO transition.

We comment on difficulty in estimating the CO gap amplitude in θ -Rb. In general, the gap amplitude may be estimated by fitting with a temperature-dependent gap model assuming a BCS-type gap function [27]. However, the large hysteresis makes fitting analysis difficult.

We now turn to the results of θ -Cs. Figures 4(a) and 4(b) show $\Delta R/R$ for $\theta = 0^\circ, 45^\circ, 90^\circ,$ and 135° . At $T = 255$ K, $\Delta R/R$ changes depending on θ . When temperature decreases to $T = 60$ K, the amplitude becomes large. Figures 4(c) and 4(d) show polar plots of the amplitude at $T = 60$ and 260 K, respectively. At both temperatures, the signal was found to be most enhanced along the c axis, similar to θ -Rb. The decomposed data are plotted in Figs. 4(e) and 4(f). The isotropic dynamics increases with decreasing temperature,

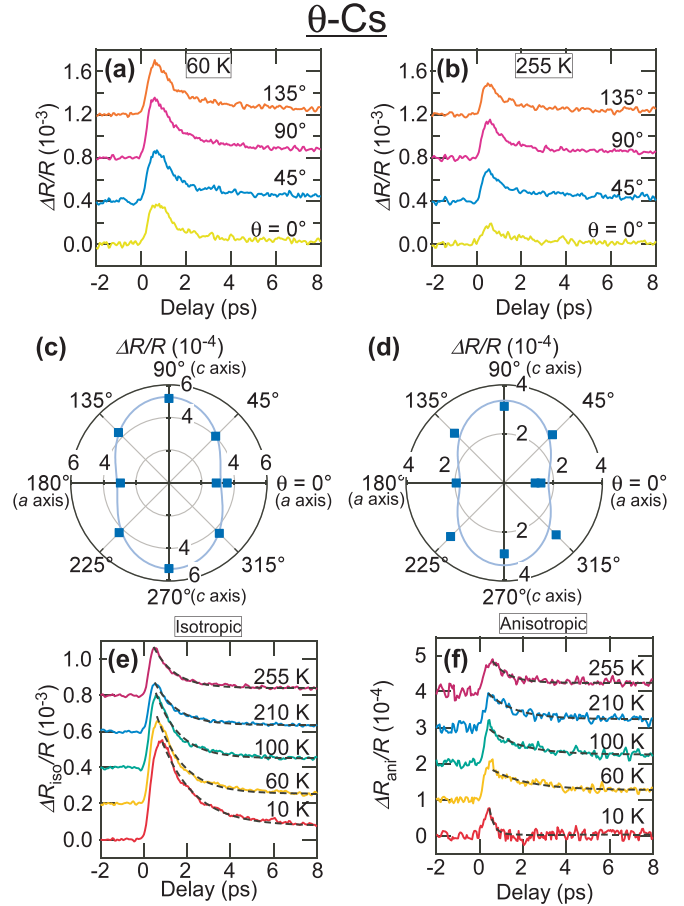


FIG. 4. (a, b) Transient change of reflectivity $\Delta R/R$ for $\theta = 0^\circ, 45^\circ, 90^\circ,$ and 135° at $T = 60$ K and 260 K, respectively, in θ -Cs. The data are shifted for clarity. (c, d) Polar plots of the amplitude of $\Delta R/R$ as a function of θ at $T = 60$ K and 255 K, respectively. The signal amplitude is defined as the $\Delta R/R$ value at 0.5 ps. The solid lines denote the results fitted by Eq. (2). (e, f) $\Delta R_{\text{iso}}/R$ and $\Delta R_{\text{ani}}/R$, respectively, at $T = 10, 60, 100, 210,$ and 255 K. The data are shifted for clarity.

but, strikingly, the anisotropic dynamics seems to remain unchanged. The θ_0 value is $\sim 90^\circ$, which is considered to be same as that in θ -Rb and is independent of temperature above ~ 50 K, as mentioned later, the anisotropic component with long relaxation time significantly decreases, so the fitting yields a large error bar in θ_0 .

Figure 5(a) shows the temperature dependencies of A_{iso} and A_{ani} on heating. As temperature decreases, A_{iso} increases monotonically but A_{ani} slightly decreases below $T_{\text{nco}} = 150$ K. On cooling as shown in Fig. 5(d), similar behaviors are also observed below T_{nco} , indicating no hysteresis. The increase in A_{iso} is similar to that in θ -Rb, indicating the formation of the CO. However, in stark contrast to θ -Rb, A_{ani} does not increase with decreasing temperature, and at first glance, the CO does not appear to involve an anisotropic change in electronic structure. As will be referred later, the behavior is related to the short-range CO domains with different orientations and the polarization anisotropy response is observed to be averaged.

Figures 5(b) and 5(e) show the temperature dependencies of τ_{iso} and τ_{ani} in the heating and cooling process, respectively.

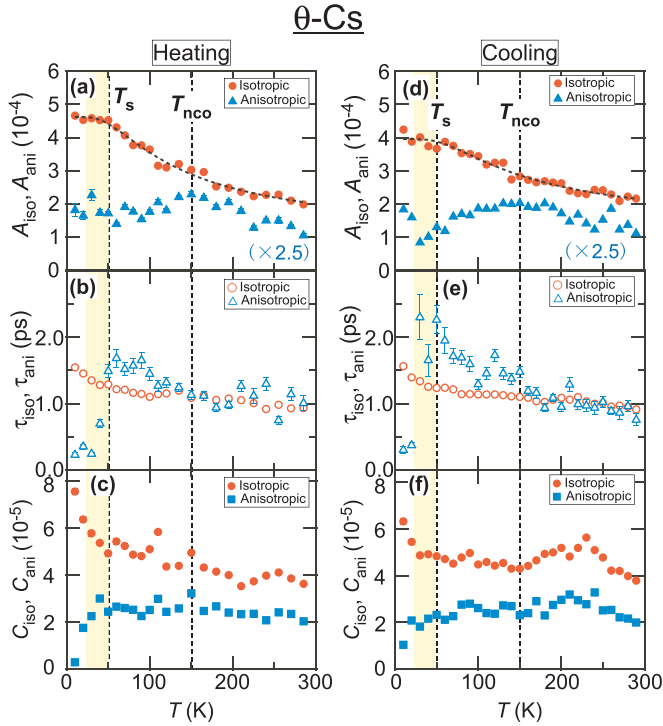


FIG. 5. (a, b, c) Temperature dependencies of A_{iso} , A_{ani} and τ_{iso} , τ_{ani} and C_{iso} , C_{ani} , respectively, on heating in θ -Cs. These on cooling are shown in panels (d, e, f).

Below T_{nco} , the gradual increase in τ_{ani} is observed. This behavior indicates that the phonon bottleneck effect becomes dominant due to opening of an energy gap. However, the steep change in decay times which is observed only on heating in θ -Rb is not observed just below T_{nco} , indicating that the first-order phase transition does not occur. These findings are consistent with that appearance of the multiple CO domains. Indeed, T_{nco} roughly corresponds to the temperature where two kinds of short-range CO develop [18,31,34].

The τ_{iso} and τ_{ani} values are ~ 1 – 2 ps in θ -Cs, which are smaller than those of ~ 2 – 3 ps in θ -Rb at low temperatures. In general, as the amplitude of the gap decreases, the bottleneck becomes more dominant, leading to the relation $\tau \sim 1/\Delta_{\text{gap}}$. Thus, the fast relaxation in θ -Cs may be reasonable because the gap amplitude will be smaller than that in the long-range CO.

Here, we estimate the gap amplitudes (Δ_{gap}) associated with multiple CO domains. In this case, the temperature-independent gap model may be applicable because the emergence temperature of CO domains is somewhat ambiguity [27]. In the model, the temperature dependence of signal amplitude is described as

$$F(T) \propto \left[1 + g \exp\left(-\frac{\Delta_{\text{gap}}}{k_B T}\right) \right]^{-1}, \quad (3)$$

where g and k_B are a variable constant and the Boltzmann constant, respectively. This model assumes a weak excitation approximation. The data of the isotropic component are fitted well as shown in Figs. 5(a) and 5(d), and the fit yields $\Delta_{\text{gap}} \approx 15$ meV on heating and 19 meV on cooling. These

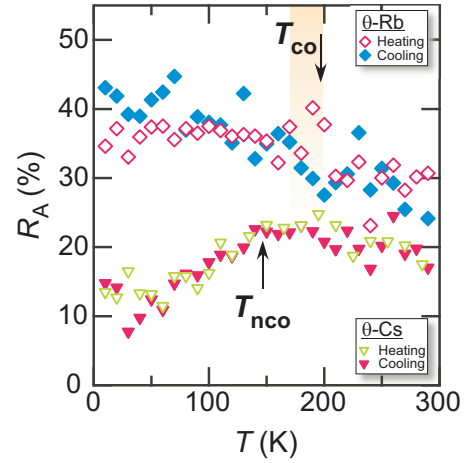


FIG. 6. Temperature dependencies of R_A in θ -Rb and θ -Cs, where R_A are defined as $A_{\text{ani}}/(A_{\text{ani}} + A_{\text{iso}})$.

values are quite smaller than the long-range CO gap [35] and comparable to the collective excitation energy of short-range CO [36].

Figures 5(c) and 5(d) show the temperature dependencies of C_{iso} and C_{ani} on heating and cooling, respectively. The C_{iso} and C_{ani} are almost independent of temperature, indicating that the lattice deformation does not occur at T_{nco} .

The anisotropic component seems to have a longer rise time at lower temperatures. Roughly estimated, the change is about 0.1 ps. However, this is shorter than the pulse duration in our measurements, making further discussion difficult.

The observed changes in the dynamics for θ -Rb and θ -Cs are distinctively characterized by a ratio of the anisotropic component, which is defined as $R_A = A_{\text{ani}}/(A_{\text{ani}} + A_{\text{iso}})$. Figure 6 shows the temperature dependencies of R_A in θ -Rb and θ -Cs. In θ -Rb, R_A increases slightly below T_{co} , meaning that the temperature dependence of A_{iso} is quite similar to that of A_{ani} . In this case, a spatial anisotropy induced by the CO is uniform over long distances in real space. In θ -Cs, however, R_A decreases below T_{nco} with decreasing temperature. This change is reflected by the fact that A_{iso} increases monotonically but A_{ani} changes little below T_{nco} , suggesting that multiple short-range CO domains appear in real space with different orientations and the anisotropy becomes weaker on average at low temperatures.

Another characteristic temperature is found at $T_s \approx 50$ K as shown in Figs. 5(b)–5(f). To highlight the low temperature region, the temperature dependencies on a logarithmic scale are shown in Figs. 7(a)–7(e). As shown in Figs. 7(a) and Figs. 7(b), in both heating and cooling processes, A_{iso} increased monotonically, but A_{ani} decreased slightly, below T_{nco} . This behavior indicates that multiple short-range CO domains appear. Below T_s , A_{iso} and A_{ani} became almost constant.

However, τ_{ani} decreased steeply at T_s , whereas τ_{iso} increased gradually with decreasing temperature, as shown in Fig. 7(b). Figure 7(c) shows the temperature dependence of C_{iso} and C_{ani} on heating. Moreover, we observed that C_{ani} decreased whereas C_{iso} increased below T_s , as the temperature decreased. The similarity between the temperature dependencies of τ_{ani} and C_{ani} indicates that, essentially, the long-lived

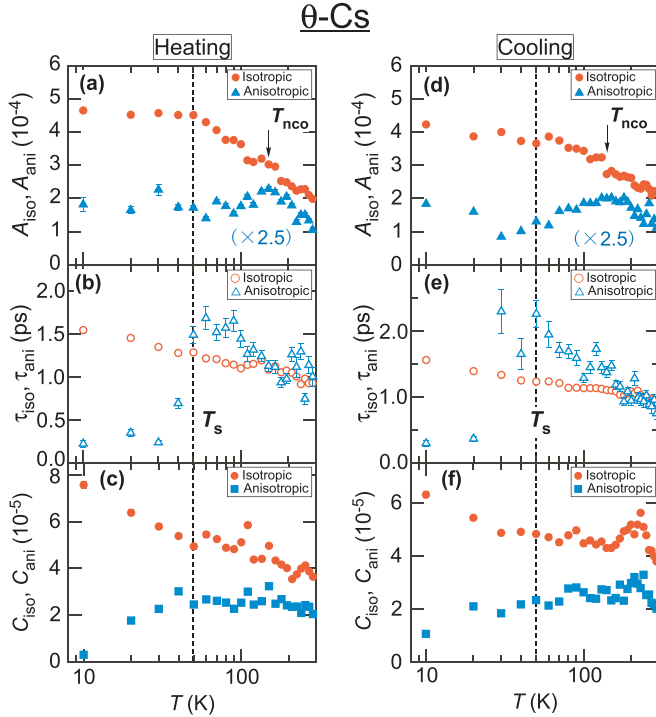


FIG. 7. (a, b, c) Temperature dependencies of A_{iso} , A_{ani} and τ_{iso} , τ_{ani} and C_{iso} , C_{ani} , respectively, on a logarithmic scale on heating in θ -Cs. These on cooling are shown in panels (d, e, f).

anisotropic dynamics decreases at T_s and disappears at low temperatures. In the cooling process, as shown in Figs. 7(e) and 7(f), the decreases in τ_{ani} and C_{ani} were also observed.

The observed changes in the dynamics at T_s are characterized by the fraction of the long-lived anisotropic component defined as $R_C = C_{\text{ani}}/(C_{\text{ani}} + C_{\text{iso}})$. Figure 8(a) shows the temperature dependence of R_C in θ -Rb for comparison. The R_C values are almost constant below T_s , indicating that the temperature dependence of C_{iso} is quite similar to that of C_{ani} , as shown in the inset of Fig. 8(a). In θ -Cs, however, R_C decreases below T_s . This is attributed to the decrease in C_{ani} and the increase in C_{iso} . The decrease in R_C is qualitatively similar to that in R_A at T_{nco} , where multiple COs are formed in a short-range with different orientations.

IV. DISCUSSION

We have shown the temperature dependencies of photoinduced carrier dynamics for θ -Rb and θ -Cs. In θ -Rb, the polarization anisotropy response is kept below T_{co} , while it decreases below T_{nco} in θ -Cs. In the following, we show that the observed dynamics arises from the long-range CO states in θ -Rb. Based on the discussion in θ -Rb, an origin of the anomalous decrease in polarization anisotropy response of θ -Cs will be discussed. In addition, we will discuss why the long-lived anisotropic dynamics are suppressed below T_s .

A. θ -Rb

First, in terms of the excitation process by the pump pulse, we refer to the origin of anisotropic dynamics that depend on

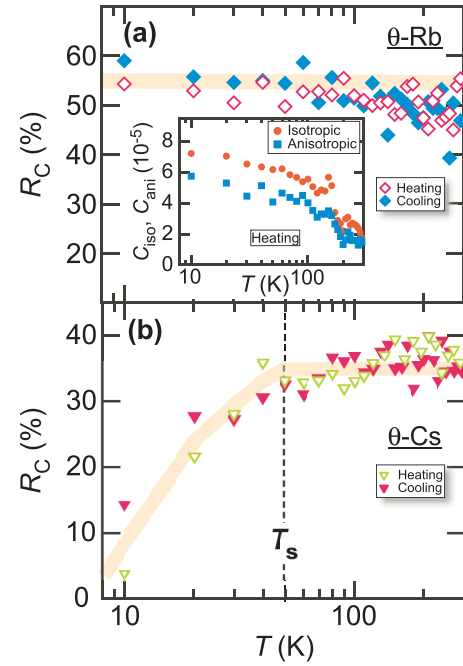


FIG. 8. (a, b) Temperature dependencies of R_C where R_C are defined as $C_{\text{ani}}/(C_{\text{ani}} + C_{\text{iso}})$ in θ -Rb and θ -Cs, respectively. The inset of panel (a) shows the temperature dependencies of C_{iso} and C_{ani} on heating in θ -Rb.

the probe polarization and isotropic dynamics that do not depend on it. There are two types of the pump excitation process; one is stimulated Raman excitation (SRE) and another is dissipative excitation (DE). In the former, carriers are coherently excited via a virtual state and keep the information of pump light, such as polarization. Thus, anisotropic excitations can occur in the SRE and, as a result, polarization anisotropy of the probe should depend on the pump polarization. In the latter case, however, the pump-excited carriers release their energy into phonons by inelastic scattering and immediately relax to a state on the gap, indicating that information of pump pulse is lost during relaxation. In the DE process, therefore, the pump excitation does not induce any anisotropic excitations, leading to only isotropic responses for the probe [37].

For the pump probe measurements, the description of the DE process is considered suitable. Indeed, in the cuprate $\text{Bi}_2\text{Sr}_2\text{CaCu}_2\text{O}_{8+\delta}$ (Bi2212) [30] and organic superconductors [38], the polarization anisotropy for the probe does not depend on pump polarization, indicating that the DE process is dominant. Moreover, superconducting (SC) and pseudogap excitations have been observed in the isotropic channel.

However, the SC excitation has been also observed in the anisotropic channel which is enhanced along the a axis in Bi2212 [30]. Since any anisotropic responses are not expected in the DE process, the observed anisotropy for the probe is induced by a rotational symmetry breaking of a system [30]. In Bi2212, the SC transition is considered to cause an anisotropy in the electronic structure which is related to a stripe-like charge ordering oriented along the Cu-O bonds [39–42].

Based on the above discussion, it is reasonable to assume that the DE process is dominant in the present measurements. As shown in Figs. 3(a) and 3(d), A_{iso} increases below T_{co} . The

resistivity measurements show a metal-insulator transition at T_{co} . This behavior is consistent with formation of an insulating gap due to the CO transition. Moreover, as shown in Fig. 6, the R_A values are almost constant below T_{co} , indicating that the CO response appears in the anisotropic channel as well as the isotropic channel. This is reasonable because electrons aligned along the c axis in the CO state leads to rotational symmetry breaking in an electronic system. We note that the probe polarization anisotropy is not directly related to anisotropy of the low-energy electronic gap structure because it is observed as a consequence of the anisotropy of the optical transition matrix elements shown in Eq. (1) [29].

In θ -Rb, the polarization anisotropy, which is enhanced along the c axis, is already present above T_{co} and the relaxation time of its dynamics is somewhat shorter than those below T_{co} . This fast relaxation is attributed to the metallic relaxation component and the polarization anisotropy arises from a structural relaxation of the lattice. When the sample is slowly cooled at a rate of less than 1 K/min [14,16] from a room temperature, the long-range CO transition occurs with the charge modulation wave vector $\mathbf{q}_2 = (0, k, 1/2)$. As a result, the polarization-dependent transient signal is more enhanced along the c axis and grows with decreasing temperature as shown in Fig. 2(c). This suggests that the dynamics arising from the long-range CO state has the same polarization anisotropy as the metallic component dominated above T_{co} .

Only on heating, the discontinuous changes in A_{iso} (A_{ani}) and τ_{iso} (τ_{ani}) are observed at $T = 160$ K and 195 K as shown in Figs. 3(a) and 3(b). The similar hysteresis has been observed in other measurements, indicating that the CO transition is the first-order [33]. In the conductance and dielectric permittivity measurements [43] as temperature increases at $T = 160$ K after rapid cooling at a rate of 4–5 K/min. or faster, the conductance and the real part of dielectric permittivity steeply change close to those obtained after slow cooling at a rate of 0.1 K/min. This indicates the transition from a metastable CO state in which a short-range CO occurs with somewhat different orientations toward the c axis direction, to a more homogeneous CO state over long distances. In our measurements, when the sample was cooled at a rate of ~ 0.5 K/min, a major part of the sample becomes the long-range CO state, but the other part remains the metastable state. As a result, the metastable CO state changes to the stable CO state at $T = 160$ K with increasing temperature. As temperature increases further, the transition from the long-range CO state to a metallic state occurs at T_{co} . These changes in electronic state can lead to abrupt changes in A_{iso} and A_{ani} at $T = 160$ K and 195 K.

An increase of τ , which is similar to our result shown in Figs. 3(b), has been often observed just below the transition temperature (T_c) in the second order phase transition, such as SC [6,7] and CDW transitions [20,44–46]. Just below T_c , the electronic ordering grows in long range, but the spatial fluctuation of the order becomes quite large, and thereby the energy gap is very small. In this case, the relaxation bottleneck effect becomes quite dominant. The excited carriers in states above the gap are relaxed to states below the gap by energy transfer to phonons. Simultaneously, phonons with energies higher than the energy gap excite the carriers back to a state higher than the gap [27,28]. As a result, the relaxation time becomes longer just below T_c . Although the CO transition is

the first order, the long-range CO state is realized between 160 and 195 K on heating, where the spatial fluctuation of the CO is expected to be dominant. This situation is considered to be similar to that just below T_c in the second order phase transition. Therefore, the increase of τ can be explained by the relaxation bottleneck due to the spatial fluctuation of the long-range CO. In this way, both isotropic and anisotropic dynamics growing below T_{co} are reasonably interpreted as the formation of the CO state.

We mention an origin of the long-lived component. A possibility is localized (intragap) states which may arise from intrinsic defect states [47]. However, since organic salts are a good candidate for the clean system, such defect states are unlikely to occur. Another possibility is lattice distortion due to electron-phonon coupling. In general, pump excitation can cause lattice distortions due to the Frank-Condon principle and its structural relaxation leads to dynamics with longer decay times than other carrier relaxation dynamics [48]. As shown in Figs. 3(c) and 3(f), the temperature dependencies of C_{iso} and C_{ani} are similar to those of A_{iso} and A_{ani} , indicating the changes in C_{iso} and C_{ani} are caused by the CO transition. The CO transition is accompanied by the lattice distortion along the same direction of the charge modulation wave vector [17]. Upon irradiation of the pump pulse, the lattice distortion caused by the CO transition is transiently modulated and recovers with time. Such structural relaxation takes a longer time than the carrier relaxation involved in the CO gap formation. In this way, the long-lived component is linked to the lattice system.

B. θ -Cs

In θ -Cs, as shown in Fig. 6, the most intriguing feature of the observed dynamics is the decrease in R_A below T_{nco} . This means that the temperature dependence of the anisotropic dynamics is different from that of the isotropic dynamics as shown in Figs. 5(a) and 5(d). Such difference has never been observed in the SC [30] and CDW transitions [20] as well as the CO transition in θ -Rb.

θ -Cs is more geometrically frustrated than θ -Rb, and more complex ground states are expected. Theoretical studies have suggested that geometrical frustration in strong Coulomb repulsions plays an important role for inducing various types of CO patterns such as horizontal, vertical and threefold types, and their degeneracies [49–51]. Experimentally, below $T \sim 160$ K which is close to T_{nco} , the x-ray diffuse scattering measurements have shown two kinds of short-range CO domains with wave vectors $\mathbf{q}_1 = (2/3, k, 1/3)$ and $\mathbf{q}_2 = (0, k, 1/2)$ [18]. The optical conductivity and Raman spectroscopy measurements have also suggested a short-range CO with small amplitude [25]. Therefore, it is plausible to consider that multiple COs appear forming a spatial domain structure. Since our pump probe spectroscopy measurement of θ -Rb were found to be sensitive to CO formation, the anomalous changes in dynamics at T_{nco} can be related to such complex CO formation in θ -Cs.

In our measurement setup, the pulse beam spot size is ~ 12 μm , which is much greater than the CO domain size of ~ 5 – 7 nm [18]. Thus, photoinduced dynamics arising from the short-range CO states can be observed as an average

of the domain structure. In the present results, the increase in the isotropic component A_{iso} with decreasing temperature is reasonably understood by growth of the CO amplitude. Moreover, the short-range COs with different directions can induce different anisotropic change in the electronic structure in each domain, leading to different signs and amplitude of transient signal. Therefore, in our measurements, such spatial dependent photoinduced anisotropy should average out, which appears to be homogeneous. As a result, no significant change is observed in A_{ani} below T_{nco} .

Contrast to θ -Rb, the long-lived components of C_{iso} and C_{ani} were found not to change significantly at T_{nco} with changing temperature in θ -Cs, indicating that the lattice modulation does not occur. Since the short-range CO domains are distributed with different orientations in θ -Cs, the energy gain in the electronic system is considered to be smaller than that of the long-range CO. As a result, the loss of the elastic energy in the lattice system may exceed the gain in electronic system, leading to no lattice distortion.

Strikingly, the long-lived anisotropic dynamics suppressed below $T_s \approx 50$ K. In the following, we discuss its origin. As we have seen, CO formation, uniform or nonuniform, has been observed to contribute to the fast decay component. Therefore, it is unlikely that CO-related changes, such as the three-dimensional ordering of CO at low temperatures [18,31] and the theoretically suggested charge-ordered liquid state called pinball liquid [50], are the origin of the disappearance of the long-lived anisotropic dynamics.

In θ -Rb, temperature changes in C_{iso} and C_{ani} are observed at T_{co} as a result of the lattice distortion, while in θ -Cs, they are not observed at T_{nco} due to the absence of lattice distortion. The findings lead to the idea that the disappearance of long-lived anisotropic dynamics below T_s should incorporate the interaction between the electronic and lattice systems. Thomas *et al.* has suggested that a glasslike structural transition of terminal ethylene groups of the BEDT-TTF molecule plays a role in the CG formation [52]. Generally, terminal ethylene groups have two types of conformation: eclipse and staggered. Thermal fluctuations occur at high temperatures, but as the temperature decreases, they are ordered in a short-range, and randomly frozen, leading to the structural transition. Such randomness can affect the electronic structure through strong charge-lattice interactions, making it more isotropic. However, the temperature at which the structural transition occurs is $T \approx 100$ K [52], which is about two times higher than T_s , suggesting that the structural transition of the ethylene groups is not directly related to the disappearance of anisotropic dynamics.

As a remaining possibility, we therefore propose that the lattice of the BEDT-TTF, and/or anion molecules is randomly deformed to match the inhomogeneous charge distribution of the CG state due to the charge-lattice coupling. Such structural deformation will provide random modulation in the electronic structure, making it more isotropic than at high temperatures. As a result, the long-lived anisotropic dynamics will no longer be observed below T_s , leading to a decrease in R_C . Moreover, the similarity between the temperature dependencies of R_C and R_A can be reasonably explained within the scenario because the modulation of the lattice is similar to that of the charge distribution.

Recent thermal conductivity measurements have revealed glasslike phonon properties at low temperatures [53]. This is one example of strong charge-lattice coupling and, simultaneously, suggests that the lattice reflects inhomogeneous charge distribution in the CG state. In our scenario, the lattice is expected to modulate to match the glassy charge distribution. Thus, the glassy phonon properties may be naturally explained as a consequence of random modulation in the lattice system.

In spin-frustrated systems, unconventional phase transitions and magnetic ground states have been suggested. Among them, a lock-in transition is accompanied by lattice distortion due to spin-lattice coupling [54]. In this transition, energy gain due to the increase in entropy in free energy plays an important role. This idea is applicable to charge-frustrated systems. The entropy of the slightly disordered lattice is expected to be greater than that of the normal lattice. However, a slight distortion leads to an increase in elastic energy. Thus, when the gain due to the entropy increase exceeds the loss of the lattice energy in the free energy at T_s , lattice deformation is expected to occur as a result of the charge-lattice coupling.

In our scenario, the lattice is irregularly deformed. Thus, it may be difficult to detect such random modulations with x-ray scattering measurements because x-ray measurements can reveal regular periodic structures in crystals. Moreover, the lattice deformation induces changes in electronic structure, whose contribution is expected to be smaller than CO-related changes. Indeed, at $T = 50$ K, the resistivity does not change significantly [16,24]. The pump probe measurement is quite sensitive to changes in low energy electronic structures. Thus, the lattice-induced change in the electronic structure could be observed through measurements of photo-excited carrier relaxation dynamics.

As shown in Figs. 7(b)–7(f), T_s may be different for descending and ascending temperature processes. It remains unclear whether or not this difference is due to hysteresis at the first-order transition because no other measurement shows such hysteresis at around T_s . Another possible origin is the inhomogeneity in real space. In the measurements presented here, the beam irradiation position on heating is different from that on cooling. If inhomogeneity occurs on a scale comparable to the beam spot size below T_s , then a different temperature dependence is expected depending on the position. In this case, a crossover rather than a structural transition may occur.

V. CONCLUSION

By conducting polarization-resolved ultrafast pump probe spectroscopy measurements, we successfully identify the nonequilibrium carrier relaxation of the long-range CO formation in θ -Rb and multiple short-range CO formations in θ -Cs. In θ -Rb, both isotropic and anisotropic dynamics changes with a hysteresis at around $T_{\text{co}} = 195$ K, indicating that the long-range CO is formed homogeneously. However, in θ -Cs, below $T_{\text{nco}} \approx 150$ K, the isotropic component increases monotonically but the anisotropic one does not change with decreasing temperature. This difference between isotropic and anisotropic dynamics is a result of the average observation of multiple short-range CO domains in different directions. In addition, we found that, in θ -Cs, the long-lived anisotropic dynamics disappear whereas the isotropic

dynamics gradually increase below $T_s \approx 50$ K, indicating that the system becomes more isotropic at low temperatures. This behavior shows the random structural transition that deforms the lattice, reflecting the inhomogeneous charge distribution in the CG state due to the charge-lattice coupling.

ACKNOWLEDGMENTS

The authors thank S. Ono for helpful discussion. This work was supported by the JCG-S Scholarship Foundation and JSPS KAKENHI Grants No. JP19K03706 and No. JP22H01162.

- [1] A. H. Zewail, Femtochemistry, *J. Phys. Chem.* **97**, 12427 (1993).
- [2] W. H. Knox, C. Hirleimann, D. A. B. Miller, J. Shah, D. S. Chemla, and C. V. Shank, Femtosecond Excitation of Nonthermal Carrier Populations in GaAs Quantum Wells, *Phys. Rev. Lett.* **56**, 1191 (1986).
- [3] M. Fiebig, K. Miyano, Y. Tomioka, and Y. Tokura, Visualization of the local insulator-metal transition in $\text{Pr}_{0.7}\text{Ca}_{0.3}\text{MnO}_3$, *Science* **280**, 1925 (1998).
- [4] Y. Tokura, Photoinduced phase transition: A tool for generating a hidden state of matter, *J. Phys. Soc. Jpn.* **75**, 011001 (2006).
- [5] S. G. Han, Z. V. Vardeny, K. S. Wong, O. G. Symko, and G. Koren, Femtosecond Optical Detection of Quasiparticle Dynamics in High- T_c $\text{YBa}_2\text{Cu}_3\text{O}_{7-\delta}$ Superconducting Thin Films, *Phys. Rev. Lett.* **65**, 2708 (1990).
- [6] D. Mihailovic, B. Podobnik, J. Demsar, G. Wagner, and J. Evetts, Divergence of the quasiparticle lifetime with doping and evidence for pre-formed pairs below T^* in $\text{YBa}_2\text{Cu}_3\text{O}_{7+\delta}$: Direct measurements by femtosecond time-resolved spectroscopy, *J. Phys. Chem. Solids* **59**, 1937 (1998).
- [7] J. Demsar, B. Podobnik, V. V. Kabanov, T. Wolf, and D. Mihailovic, Superconducting Gap Δ_c , the Pseudogap Δ_p , and Pair Fluctuations Above T_c in Overdoped $\text{Y}_{1-x}\text{Ca}_x\text{Ba}_2\text{Cu}_3\text{O}_{7-\delta}$ from Femtosecond Time-Domain Spectroscopy, *Phys. Rev. Lett.* **82**, 4918 (1999).
- [8] R. A. Kaindl, M. Woerner, T. Elsaesser, D. C. Smith, J. F. Ryan, G. A. Farnan, M. P. McCurry, and D. G. Walmsley, Ultrafast mid-infrared response of $\text{YBa}_2\text{Cu}_3\text{O}_{7-\delta}$, *Science* **287**, 470 (2000).
- [9] Y. H. Liu, Y. Toda, K. Shimatake, N. Momono, M. Oda, and M. Ido, Direct Observation of the Coexistence of the Pseudogap and Superconducting Quasiparticles in $\text{Bi}_2\text{Sr}_2\text{CaCu}_2\text{O}_{8+y}$ by Time-Resolved Optical Spectroscopy, *Phys. Rev. Lett.* **101**, 137003 (2008).
- [10] T. Mertelj, V. V. Kabanov, C. Gadermaier, N. D. Zhigadlo, S. Katrych, J. Karpinski, and D. Mihailovic, Distinct Pseudogap and Quasiparticle Relaxation Dynamics in the Superconducting State of Nearly Optimally Doped $\text{SmFeAsO}_{0.8}\text{F}_{0.2}$ Single Crystals, *Phys. Rev. Lett.* **102**, 117002 (2009).
- [11] T. Mertelj, P. Kusar, V. V. Kabanov, L. Stojchevska, N. D. Zhigadlo, S. Katrych, Z. Bukowski, J. Karpinski, S. Weyeneth, and D. Mihailovic, Quasiparticle relaxation dynamics in spin-density-wave and superconducting $\text{SmFeAsO}_{1-x}\text{F}_x$ single crystals, *Phys. Rev. B* **81**, 224504 (2010).
- [12] T. Naito, Y. Yamada, T. Inabe, and Y. Toda, Carrier dynamics in κ -type organic superconductors: Time-resolved observation, *J. Phys. Soc. Jpn.* **77**, 064709 (2008).
- [13] Y. Toda, T. Mertelj, T. Naito, and D. Mihailovic, Femtosecond Carrier Relaxation Dynamics and Photoinduced Phase Separation in κ -(BEDT-TTF) $_2$ Cu[N(CN) $_2$]X (X = Br, Cl), *Phys. Rev. Lett.* **107**, 227002 (2011).
- [14] F. Kagawa, T. Sato, K. Miyagawa, K. Kanoda, Y. Tokura, K. Kobayashi, R. Kumai, and Y. Murakami, Charge-cluster glass in an organic conductor, *Nat. Phys.* **9**, 419 (2013).
- [15] S. Sasaki, K. Hashimoto, R. Kobayashi, K. Itoh, S. Iguchi, Y. Nishio, Y. Ikemoto, T. Moriwaki, N. Yoneyama, M. Watanabe, A. Ueda, H. Mori, K. Kobayashi, R. Kumai, Y. Murakami, J. Muller, and T. Sasaki, Crystallization and vitrification of electrons in a glass-forming charge liquid, *Science* **357**, 1381 (2017).
- [16] H. Mori, S. Tanaka, and T. Mori, Systematic study of the electronic state in θ -type BEDT-TTF organic conductors by changing the electronic correlation, *Phys. Rev. B* **57**, 12023 (1998).
- [17] M. Watanabe, Y. Noda, Y. Nogami, and H. Mori, Transfer integrals and the spatial pattern of charge ordering in θ -(BEDT-TTF) $_2$ RbZn(SCN) $_4$ at 90 K, *J. Phys. Soc. Jpn.* **73**, 116 (2004).
- [18] T. Sato, F. Kagawa, K. Kobayashi, K. Miyagawa, K. Kanoda, R. Kumai, Y. Murakami, and Y. Tokura, Emergence of nonequilibrium charge dynamics in a charge-cluster glass, *Phys. Rev. B* **89**, 121102(R) (2014).
- [19] T. Sato, F. Kagawa, K. Kobayashi, A. Ueda, H. Mori, K. Miyagawa, K. Kanoda, R. Kumai, Y. Murakami, and Y. Tokura, Systematic variations in the charge-glass-forming ability of geometrically frustrated θ -(BEDT-TTF) $_2$ X organic conductors, *J. Phys. Soc. Jpn.* **83**, 083602 (2014).
- [20] S. Tsuchiya, Y. Sugawara, S. Tanda, and Y. Toda, Symmetry-dependent carrier relaxation dynamics and charge-density-wave transition in DyTe_3 probed by polarized femtosecond spectroscopy, *J. Opt.* **17**, 085501 (2015).
- [21] S. Tsuchiya, K. Nakagawa, J. Yamada, H. Taniguchi, and Y. Toda, Photoinduced phase separation with local structural ordering in organic molecular conductors, *Phys. Rev. B* **96**, 134311 (2017).
- [22] K. Nakagawa, S. Tsuchiya, J. Yamada, and Y. Toda, Fluctuating superconductivity in κ -type organic compounds probed by polarized time-resolved spectroscopy, *Europhys. Lett.* **122**, 67003 (2018).
- [23] F. Kagawa and H. Oike, Quenching of charge and spin degrees of freedom in condensed matter, *Adv. Mater.* **29**, 1601979 (2017).
- [24] T. Sato, K. Miyagawa, M. Tamura, and K. Kanoda, Anomalous 2D-Confined Electronic Transport in Layered Organic Charge-Glass Systems, *Phys. Rev. Lett.* **125**, 146601 (2020).
- [25] K. Suzuki, K. Yamamoto, K. Yakushi, and A. Kawamoto, Infrared and Raman studies of θ -(BEDT-TTF) $_2$ CsZn(SCN) $_4$: Comparison with the frozen state of θ -(BEDT-TTF) $_2$ RbZn(SCN) $_4$, *J. Phys. Soc. Jpn.* **74**, 2631 (2005).

- [26] P. B. Allen, Theory of Thermal Relaxation of Electrons in Metals, *Phys. Rev. Lett.* **59**, 1460 (1987).
- [27] V. V. Kabanov, J. Demsar, B. Podobnik, and D. Mihailovic, Quasiparticle relaxation dynamics in superconductors with different gap structures: Theory and experiments on $\text{YBa}_2\text{Cu}_3\text{O}_{7-\delta}$, *Phys. Rev. B* **59**, 1497 (1999).
- [28] A. Rothwarf and B. N. Taylor, Measurement of Recombination Lifetimes in Superconductors, *Phys. Rev. Lett.* **19**, 27 (1967).
- [29] D. Dvorsek, V. V. Kabanov, J. Demsar, S. M. Kazakov, J. Karpinski, and D. Mihailovic, Femtosecond quasiparticle relaxation dynamics and probe polarization anisotropy in $\text{YSr}_x\text{Ba}_{2-x}\text{Cu}_4\text{O}_8$ ($x = 0, 0.4$), *Phys. Rev. B* **66**, 020510(R) (2002).
- [30] Y. Toda, F. Kawanokami, T. Kurosawa, M. Oda, I. Madan, T. Mertelj, V. V. Kabanov, and D. Mihailovic, Rotational symmetry breaking in $\text{Bi}_2\text{Sr}_2\text{CaCu}_2\text{O}_{8+\delta}$ probed by polarized femtosecond spectroscopy, *Phys. Rev. B* **90**, 094513 (2014).
- [31] Y. Nogami, J.-P. Pouget, M. Watanabe, K. Oshima, H. Mori, S. Tanaka, and T. Mori, Structural modulation in θ -(BEDT-TTF) $_2\text{CsM}(\text{SCN})_4$ [$M = \text{Co}, \text{Zn}$], *Synth. Met.* **103**, 1911 (1999).
- [32] M. Watanabe, Y. Noda, Y. Nogami, and H. Mori, Investigation of x-ray diffuse scattering in θ -(BEDT-TTF) $_2\text{RbM}(\text{SCN})_4$, *Synth. Met.* **135**, 665 (2003).
- [33] T. Takeno, K. Kobayashi, Y. Nishio, K. Kajita, H. Mori, and T. Nakamura, Mysterious charge ordering on θ -(BEDT-TTF) $_2\text{RbZn}(\text{SCN})_4$, *J. Phys.: Conf. Ser.* **150**, 042201 (2009).
- [34] M. Watanabe, Y. Nogami, K. Oshima, H. Mori, and S. Tanaka, Novel pressure-induced $2k_F$ CDW state in organic low-dimensional compound θ -(BEDT-TTF) $_2\text{CsCo}(\text{SCN})_4$, *J. Phys. Soc. Jpn.* **68**, 2654 (1999).
- [35] K. Hashimoto, R. Kobayashi, S. Ohkura, S. Sasaki, N. Yoneyama, M. Suda, H. M. Yamamoto, and T. Sasaki, Optical conductivity spectra of charge-crystal and charge-glass states in a series of θ -type BEDT-TTF compounds, *Crystals* **12**, 831 (2022).
- [36] K. Hashimoto, S. C. Zhan, R. Kobayashi, S. Iguchi, N. Yoneyama, T. Moriwaki, Y. Ikemoto, and T. Sasaki, Collective excitation of a short-range charge ordering in θ -(BEDT-TTF) $_2\text{CsZn}(\text{SCN})_4$, *Phys. Rev. B* **89**, 085107 (2014).
- [37] H. J. Zeiger, J. Vidal, T. K. Cheng, E. P. Ippen, G. Dresselhaus, and M. S. Dresselhaus, Theory for dispersive excitation of coherent phonons, *Phys. Rev. B* **45**, 768 (1992).
- [38] K. Nakagawa, S. Tsuchiya, J. Yamada, and Y. Toda, Pump-and-probe-polarization analyses of ultrafast carrier dynamics in organic superconductors, *J. Supercond. Novel Magn.* **29**, 3065 (2016).
- [39] K. M. Lang, V. Madhavan, J. E. Hoffman, E. W. Hudson, H. Eisaki, S. Uchida, and J. C. Davis, Imaging the granular structure of high- T_c superconductivity in underdoped $\text{Bi}_2\text{Sr}_2\text{CaCu}_2\text{O}_{8+\delta}$, *Nature* **415**, 412 (2002).
- [40] C. Howald, H. Eisaki, N. Kaneko, M. Greven, and A. Kapitulnik, Periodic density-of-states modulations in superconducting $\text{Bi}_2\text{Sr}_2\text{CaCu}_2\text{O}_{8+\delta}$, *Phys. Rev. B* **67**, 014533 (2003).
- [41] M. Vershinin, S. Misra, S. Ono, Y. Abe, Y. Ando, and A. Yazdani, Local ordering in the pseudogap state of the high- T_c superconductor $\text{Bi}_2\text{Sr}_2\text{CaCu}_2\text{O}_{8+\delta}$, *Science* **303**, 1995 (2004).
- [42] Y. Kohsaka, C. Taylor, K. Fujita, A. Schmidt, C. Lupien, T. Hanaguri, M. Azuma, M. Takano, H. Eisaki, H. Takagi, S. Uchida, and J. C. Davis, An intrinsic bond-centered electronic glass with unidirectional domains in underdoped cuprates, *Science* **315**, 1380 (2007).
- [43] F. Nad, P. Monceau, and H. M. Yamamoto, Effect of cooling rate on charge ordering in θ -(BEDT-TTF) $_2\text{RbZn}(\text{SCN})_4$, *Phys. Rev. B* **76**, 205101 (2007).
- [44] J. Demsar, K. Biljaković, and D. Mihailovic, Single Particle and Collective Excitations in the One-Dimensional Charge Density Wave Solid $\text{K}_{0.3}\text{MoO}_3$ Probed in Real Time by Femtosecond Spectroscopy, *Phys. Rev. Lett.* **83**, 800 (1999).
- [45] J. Demsar, L. Forró, H. Berger, and D. Mihailovic, Femtosecond snapshots of gap-forming charge-density-wave correlations in quasi-two-dimensional dichalcogenides $1T$ - TaS_2 and $2H$ - TaSe_2 , *Phys. Rev. B* **66**, 041101(R) (2002).
- [46] R. V. Yusupov, T. Mertelj, J.-H. Chu, I. R. Fisher, and D. Mihailovic, Single-Particle and Collective Mode Couplings Associated with 1- and 2-Directional Electronic Ordering in Metallic $R\text{Te}_3$ ($R = \text{Ho}, \text{Dy}, \text{Tb}$), *Phys. Rev. Lett.* **101**, 246402 (2008).
- [47] V. V. Kabanov, J. Demsar, and D. Mihailovic, Carrier-relaxation dynamics in intragap states: The case of the superconductor and the charge-density-wave semiconductor, *Phys. Rev. B* **61**, 1477 (2000).
- [48] D. Mihailovic and J. Demsar, Time-resolved optical studies of quasiparticle dynamics in high-temperature superconductors: Experiments and theory, "Spectroscopy of Superconducting Materials," in *ACS Symposium Series*, edited by E. Faulques (American Chemical Society, Washington, DC, 1999), Vol. 730.
- [49] M. Kaneko and M. Ogata, Mean-field study of charge order with long periodicity in θ -(BEDT-TTF) $_2\text{X}$, *J. Phys. Soc. Jpn.* **75**, 014710 (2006).
- [50] C. Hotta and N. Furukawa, Strong coupling theory of the spinless charges on triangular lattices: Possible formation of a gapless charge-ordered liquid, *Phys. Rev. B* **74**, 193107 (2006).
- [51] S. Mahmoudian, L. Rademaker, A. Ralko, S. Fratini, and V. Dobrosavljević, Glassy Dynamics in Geometrically Frustrated Coulomb Liquids without Disorder, *Phys. Rev. Lett.* **115**, 025701 (2015).
- [52] T. Thomas, Y. Saito, Y. Agarmani, T. Thyzel, M. Lonsky, K. Hashimoto, T. Sasaki, M. Lang, and J. Müller, Involvement of structural dynamics in charge-glass formation in strongly frustrated molecular metals, *Phys. Rev. B* **105**, L041114 (2022).
- [53] T. Nomoto, S. Yamashita, H. Akutsu, Y. Nakazawa, and A. I. Krivchikov, Phonon glass induced by electron correlation, *J. Phys. Soc. Jpn.* **88**, 073601 (2019).
- [54] S.-H. Lee, C. Broholm, T. H. Kim, W. Ratcliff, and S.-W. Cheong, Local Spin Resonance and Spin-Peierls-Like Phase Transition in a Geometrically Frustrated Antiferromagnet, *Phys. Rev. Lett.* **84**, 3718 (2000).